International Journal of Multiphase Flow 52 (2013) 22–34

Contents lists available at SciVerse ScienceDirect

International Journal of Multiphase Flow

journal homepage: www.elsevier.com/locate/ijmulflow

Evaluation of level set and phase field methods in modeling two phase flow with viscosity contrast through dual-permeability porous medium

H.A. Akhlaghi Amiri, A.A. Hamouda *

Department of Petroleum Engineering, University of Stavanger (UiS), 4036 Stavanger, Norway

ARTICLE INFO

Article history:
Received 1 June 2012
Received in revised form 10 December 2012
Accepted 26 December 2012
Available online 4 January 2013

Keywords:
Two phase flow
Level set method
Phase field method
Viscosity
Permeability
Surface tension

ABSTRACT

This work assesses conservative level set method (LSM) and Cahn–Hilliard phase field method (PFM) in modeling 2D two-phase flow through porous media, based on their ability to capture different phenomena associated with the medium permeability and fluid viscosity contrasts. The assessment includes their accuracy and running time. For this purpose, a robust finite element solver (COMSOL Multiphysics™) is used here to do the computations. To start with, the main parameters of the methods including the interface thickness, mesh size and diffusion coefficient are studied. Rectangular bubble relaxation is simulated to compare the two methods in capturing the physics of the bubble evolution. The comparison is also made for a stratified two-phase flow and flow in different single pore elements. Two models are then constructed to simulate two-phase flow with viscosity contrast through complex porous media, including homogenous medium with obstacle and dual-permeability medium. Both methods are able to capture the basic phenomena; however PFM is more successful in capturing the physical details especially in complicated porous media, compared to LSM. PFM results such as pressure gradients and fluid profiles in the media are more realistic. While LSM is unsuccessful in volume conservation and modeling no-slip boundary conditions. In addition, the running times are considerably less for PFM in simulation of different scenarios.

1. Introduction

Understanding transport phenomena in porous media is of great importance in many fields such as petroleum engineering (Valvatne and Blunt, 2004). To better comprehend such phenomena, it is useful to model two phase flow problems at pore-scales. Pore-scale models can be used to derive macro-scale constitutive relations (e.g. capillary pressure and relative permeabilities) and to provide flow properties for simulation in larger scales (Valvatne and Blunt, 2004; Ramstad et al., 2009). Initial studies on the behavior of two-phase flow are dated back to the beginning of 19th century, when Young (1805) and other investigators developed the qualitative theory of surface tension. In recent years, a variety of two-phase flow simulation methods have been suggested that can be implemented at pore-scales, e.g., pore network modeling (Blunt, 2001), Lattice Boltzman method (Succi, 2001), front tracking method (Unverdi and Tryggvason, 1992), volume of fluid (VOF) method (Hirt and Nichols, 1981), level set method (Osher and Sethian, 1988; Smereka and Sethian, 2003), phase field method (Jacqmin, 1999; Badalassi et al., 2003) and so on. Pore-scale simulation of fluid flow through porous media demands a method that can handle complex pore geometries and topological changes. Among other methods, level set method (LSM) and phase field method (PFM), which are categorized as interface capturing approaches, are becoming increasingly popular because of their ability to accurately model flow problems involving sophisticated moving interfaces and complex topologies (Sussman et al., 1999; Yue et al., 2004). The main goal of present work is to compare these methods and find the more efficient one in solving pore-scale two phase flow problems, from accuracy and running time points of view.

LSM was first developed by Osher and Sethian (1988). It is a class of numerical techniques in which the interface evolution in space and time is modeled by an advection equation (Smereka and Sethian, 2003). The standard LSM is not volume conservative; so different combinations of the LSM with other conservative schemes have been proposed to solve this problem (e.g. LSM coupled with variable density projection method (Sussman et al., 1999) and VOF method (Sussman and Puckett, 2000)). Although these approaches improve the volume conservation of the LSM, they are not as simple as LSM itself (Olsson and Kreiss, 2005). Olsson et al. (2007) suggested a two-step LSM, which is able to conserve the volume and keep the main structure of the standard LSM.

The first idea of PFM (also known as diffuse-interface method) goes back to a century ago when van der Waals (1979) modeled a liquid–gas system using a density function that varies

* Corresponding author. Tel.: +47 51832271.
E-mail address: aly.hamouda@uis.no (A.A. Hamouda).

0301-9322/$ - see front matter © 2013 Elsevier Ltd. All rights reserved.
http://dx.doi.org/10.1016/j.ijmultiphaseflow.2012.12.006

continuously at the interface. Convective Cahn–Hilliard equation (proposed by Cahn and Hilliard (1958)) is the best known example of PFM that can conserve the volume and is relatively easy to implement in two and three dimensions (Jacqmin, 1999). During the last decade, different applications of Cahn–Hilliard PFM in simulation of two-phase Navier–Stokes flows have been suggested (Liu and Shen, 2003; Chiu and Lin, 2011; Bogdanov et al., 2010).

Both LSM and PFM compute two phase flow on a fixed Eulerian grid. In both methods the state of the entire domain is represented continuously by an indicator function (i.e., level set function in LSM and order parameter in PFM) that assumes distinct constant values in each bulk phase and undergoes rapid but smooth variation in the interfacial region (Smereka and Sethian, 2003; Yue et al., 2006). The physical fluid properties (e.g. density and viscosity) are modified in order to be constant in bulk phases and vary smoothly across the interface. The incompressible Navier–Stokes equation with variable viscosity and density is coupled with the convective equation of interface to implicitly describe the fluid dynamics in the domain (Olsson et al., 2007; Badalassi et al., 2003).

From a methodological standpoint, LSM is a computational approach in which the interface motion is numerically approximated using artificial smoothing function. While PFM is based on a physical approach which incorporates the phases and interface between them into the free energy function of the system. It means that PFM not only transports the interface with the flow but ensures that the total energy of the system is minimized correctly. The evolution of the interface therefore is self-consistent in PFM and does not need ad hoc intervention such as the re-initialization in LSM (Zhou et al., 2010). Another difference between LSM and PFM is that the choice of level set function is somewhat arbitrary, but for PFM, the exact profile of the order parameter is important in obtaining the correct interface motion (Smereka and Sethian, 2003). The advantages and limitations of PFM and LSM have been discussed more by Feng et al. (2005) and Smereka and Sethian (2003).

In present work, 2D flow problems are modeled using conservative LSM and Cahn–Hilliard PFM solved by finite-element scheme, which can accommodate complex flow geometries.

2. Theory and numerical methods

2.1. Interface equations

The level set function (ϕ_{LS}) is a numerical smoothing parameter, while the phase field orders parameter (ϕ_{PF}) is a physical quantity which represents the concentration fractions of the two phases. However, both are used to model fluid interface as having finite thickness. In this work they are defined in a way that go rapidly from zero to one across the interface, hence sharp interface is at their 0.5 contour. The main equations of the conservative LSM and Cahn–Hilliard PFM are presented in this section. More details can be obtained from works done by Olsson et al. (2005, 2007) for conservative LSM and Wheeler et al. (1995) and Yue et al. (2006) for Cahn–Hilliard PFM.

The interface evolution in the standard LSM is given by a simple numerical convection (Osher and Sethian, 1988); however it fails to conserve the volume due to the absence of diffusion term in the equation. Therefore, using numerical techniques, an artificial compression and diffusion are added in order to maintain the interface thickness (Olsson et al., 2007). The compression–diffusion equation is obtained as:

$$\frac{\partial \phi_{LS}}{\partial t} + u \cdot \nabla \phi_{LS} = \omega \nabla \cdot (\varepsilon_{ls} \nabla \phi_{LS} - \phi_{LS}(1-\phi_{LS})n) \tag{1}$$

where u is the fluid velocity field, ω is a numerical parameter (re-initialization parameter) with the dimension of velocity, ε_{LS} is a measure for the interfacial thickness in LSM and n is the interface normal vector that is easily calculated as $n = \nabla\phi_{LS}/|\nabla\phi_{LS}|$. According to Olsson et al. (2007), conservative LSM is a two step method, advective step and re-initialization step. In advective step simple convection equation is solved. The resulting ϕ_{LS} is then used as initial condition for Eq. (1) in re-initialization step.

Cahn–Hilliard convection equation is a time dependent form of the energy minimization concept. It is obtained by approximating interfacial diffusion fluxes as being proportional to chemical potential gradients, enforcing conservation of the field (Badalassi et al., 2003). This equation models creation, evolution and dissolution of the interface:

$$\frac{\partial \phi_{PF}}{\partial t} + u \cdot \nabla \phi_{PF} = \nabla \cdot (M \nabla G) \tag{2}$$

where M is the diffusion coefficient called mobility and G is the chemical potential of the system. Mobility can be expressed as $M = M_c \varepsilon_{PF}^2$, where M_c is the characteristic mobility that governs the temporal stability of diffusive transport and ε_{PF} is a capillary width that scales with the interface thickness in PFM. The chemical potential is derived from total energy equation as $G = \lambda\left[1/\varepsilon_{PF}^2 \phi_{PF}(\phi_{PF} - \frac{1}{2})(\phi_{PF} - 1) - \nabla^2 \phi_{PF}\right]$, where λ is the mixing energy density. Eq. (2) implies that the temporal evolution of ϕ_{PF} depends on convective transport due to the divergence free velocity and diffusive transport due to gradients in the chemical potential (Donaldson et al., 2011).

One dimensional equilibrium interface profile for conservative LSM is obtained as a steady solution of Eq. (1) which can be expressed as $\phi_{0LS}(x) = 1/[1 + \exp(-x/\varepsilon_{LS})]$. In the case of PFM, this equilibrium interface profile is derived by minimizing the total energy functional with respect to the variations of ϕ_{PF} (i.e., $G = 0$), which can be given by $\phi_{0PF}(x) = 0.5\left[1 + \tanh(x/\sqrt{2}\varepsilon_{PF})\right]$ (Wheeler et al., 1995). If one takes $0.05 < \phi_{LS}$ (or ϕ_{PF}) < 0.95 to be the extent of the interface, the equilibrium profiles of LSM and PFM give interfacial thicknesses of $5.889\varepsilon_{LS}$ and $4.164\varepsilon_{PF}$, respectively. So interfacial thicknesses of the two methods are equal if $\varepsilon_{PF} = \sqrt{2}\varepsilon_{LS}$. It is worth to note that the LSM and PFM interface equilibrium equations are also analytically identical when $\varepsilon_{PF} = \sqrt{2}\varepsilon_{LS}$:

$$\begin{aligned}\frac{1}{1+\exp\left(\frac{-x}{\varepsilon_{LS}}\right)} = \frac{\exp\left(\frac{x}{\varepsilon_{LS}}\right)}{1+\exp\left(\frac{x}{\varepsilon_{LS}}\right)} &= \frac{1}{2}\left[1 + \frac{\exp\left(\frac{\sqrt{2}x}{\varepsilon_{PF}}\right) - 1}{\exp\left(\frac{\sqrt{2}x}{\varepsilon_{PF}}\right) + 1}\right] \\ &= \frac{1}{2}\left[1 + \tanh\left(\frac{x}{\sqrt{2}\varepsilon_{PF}}\right)\right]\end{aligned} \tag{3}$$

2.2. Momentum equation

To simulate immiscible two phase flow problems, the interface equations are coupled with the following incompressible Navier–Stokes and continuity equations:

$$\rho(\phi)\frac{\partial u}{\partial t} + \rho(\phi)u \cdot \nabla u = -\nabla p + \nabla \cdot [\mu(\phi)(\nabla u + \nabla u^T)] + \rho(\phi)g + F_{st} \tag{4}$$

$$\nabla \cdot u = 0 \tag{5}$$

where p is pressure, ρ is density, μ is viscosity, g is gravitational acceleration, F_{st} is surface tension that is introduced as a body force in the momentum equation and ϕ can be ϕ_{LS} or ϕ_{PF}. The density and viscosity are defined as $\rho(\phi) = \rho_1 + (\rho_2 - \rho_1)\phi$ and $\mu(\phi) = \mu_1 + (\mu_2 - \mu_1)\phi$, respectively, where subscripts 1 and 2 denote two different phases.

In the case of LSM, the interfacial force can be calculated solving the following relation (Shepel and Smith, 2006):

$$F_{st,LS} = \sigma\kappa n\delta(\phi_{LS}) \quad (6)$$

where σ is the surface tension coefficient, $\kappa = -\nabla\cdot(\nabla\phi_{LS}/|\nabla\phi_{LS}|)$ is the local curvature of the interface and δ is a smoothed delta function which can be scaled with $\nabla\phi_{LS}$. In PFM, surface body force is calculated by derivation of the total free energy due to the spatial coordinate which is obtained as follows (Yue et al., 2006):

$$F_{st,PF} = G\nabla\phi_{PF} \quad (7)$$

PFM considers surface tension as an intrinsic property corresponding to the excess free energy density of the interfacial region (Qin and Bhadeshia, 2010). Surface tension coefficient for PFM is equal to the integral of the free energy density across the interface, which is $\sigma = 2\sqrt{2}\lambda/3\varepsilon_{PF}$ in the case of a planar interface.

2.3. Numerical schemes

Numerical simulations are carried out using the commercial software of COMSOL Multiphysics™, an interactive environment for modeling different scientific and engineering problems. It uses finite element method (FEM) for solving the equations. The software runs finite element analysis together with error control using a variety of numerical solvers (COMSOL Multiphysics user's guide, 2011).

Triangular mesh elements are used in all the computations in present work. To avoid unphysical distortions and to make sure about the accuracy of the results, the interface should be thin enough to approach a sharp transition. A sharp transition will imply less smearing of density, viscosity and surface tension. A small interface thickness can also result in better conservation of the area bounded by the 0.5 contour (Olsson et al., 2007). On the other hand, the interface region must be adequately resolved by fine mesh. These conditions are described in detail by Zhou et al. (2010) as model convergence and mesh convergence. In PFM, mobility is another important parameter that affects the accuracy of the method (Jacqmin, 1999). The choice of the mobility (M) is one of the subtleties of PFM. M has to be large enough to retain a more or less constant interfacial thickness and small enough to keep the convective motion (Yue et al., 2006). According to Olsson et al. (2007), the choice of re-initialization parameter (ω) in LSM needs attention, which is discussed more in coming sections. The time steps sizes are controlled by the numerical solver during the computations, using backward differentiation formulas (BDFs). Particularly, the initial time step sizes are small enough to avoid singularity.

As discussed by Yue et al. (2006), to apply finite element discretization, the fourth order derivative term in Eq. (2) needs to be divided into two second order equations using an auxiliary parameter. Therefore, the computations of LSM are done using three dependant variables of $\{u, p, \phi\}$, while PFM has the mentioned additional parameter; i.e., for the same problem, the number of degrees of freedom that are solved for LSM is less than PFM.

The interface convective equations of LSM and PFM must be initialized before time dependant solving. In the initialization step, the interface equation is solved at stationary conditions ($u = 0$) in order to ϕ vary smoothly across the initial interface. Normally, a shorter initialization time is required for LSM, compared to PFM. The influence of the initialization time on the results of the methods is more discussed in Section 3.1.

3. Results and discussions

The numerical results of different 2D problems are presented in this section to validate and compare LSM and PFM. The rectangular bubble evolution, co-current two-phase flow in the channel, two-phase flow through single pore elements, homogenous and dual-permeability porous media are the studied problems.

3.1. Rectangular bubble deformation

The bubble relaxation is driven only by the interfacial tension. Thus, it can be used to show how accurately the methods compute the interfacial force. The effects of the diffusion terms (M and ω) on the bubble area conservation are also studied. An initially rectangle bubble with the side length of l_b is simulated at the middle of a square domain with the dimension of πl_b. The viscosity ratio is defined as $\beta = \mu_2/\mu_1$, with the subscripts 1 and 2 denoting matrix and bubble, respectively. There is no externally imposed velocity so the only time scale is the capillary time $t_c = \mu_1 l_c/\sigma$, where l_c is the characteristic length. l_b is set as the characteristic length in this problem. The Cahn number is $Cn = \varepsilon/l_c$, where ε is the interface thickness parameter. To compare the two methods, we set $\varepsilon = \sqrt{2}\varepsilon_{LS}$ for LSM and $\varepsilon = \varepsilon_{PF}$ for PFM (see Section 2.1). The bulk maximum mesh element size is fixed at $0.125l_b$ and it is refined to $0.02l_b$ around the bubble region. Further refinement produces no visible change in the results. Cn is set to 0.013. Both methods predict qualitatively identical bubble profiles during the evolution in a good agreement with the literature results (Liu and Shen, 2003). The bubble oscillates until it approaches the stabilized circular bubble at $t_D = 50$. After equilibrium, small parasite currents appear especially in the neighborhood of the interfaces, which is prevalent in surface tension simulation methods. According to Renardy and Renardy (2002), the maximum parasite velocity magnitude in the computational domain is scaled with σ/μ. The parasite currents simulated by PFM and LSM are in order of $0.001\sigma/\mu$ and $0.002\sigma/\mu$, respectively, i.e., PFM demonstrates smaller parasite currents, compared to LSM. These error values are approximately one order of magnitude smaller than the values reported by Lafaurie et al. (1994), Renardy and Renardy (2002) and Dupont and Legendre (2010). This is mainly due to the robust finite element solver used in this work.

As bubble deforms, small bubble area shrinkages are predicted by the two methods. The shrinkage ratio (R_s) is defined here as R_s = (bubble area bounded by $\phi = 0.5$)/(original bubble area, l_b^2). A sensitivity analysis is made to compare the ability of PFM and LSM in conserving the volume. Shrinkage rate is found to be a function of M in PFM and ω in LSM. Mobility term (M) in PFM accounts for the diffusion-related time scale of the interface (see Eq. (2)). For LSM, it is possible to assume the re-initialization parameter (ω) as an artificial diffusion parameter (see Eq. (1)). The Péclet number is defined for PFM and LSM as $Pe_{PF} = \sigma l_b/(\mu_2 M_c\lambda)$ and $Pe_{LS} = \sigma l_b/(\mu_2\omega\varepsilon_{LS})$, respectively. The diffusion-related time scales for PFM and LSM are hence defined as $t_{dif,PF} = l_b\varepsilon_{PF}/(M_c\lambda)$ and $t_{dif,LS} = l_b/\omega$, respectively. As indicated in Section 2.3, the initialization step solves the interface equations (Eqs. (1) and (2)) at stationary conditions, i.e., pure diffusion without any convection. For a problem such as rectangular bubble evolution, this pure diffusion can cause deformations in the bubble when t_{in}/t_{dif} is large, where t_{in} is initialization time. Fig. 1 shows how a long t_{in} has resulted in diffusion-controlled shape modification in both methods, especially on the bubble corners. Since PFM interface equation (Eq. (2)) satisfies the energy minimization criterion, the bubble deformation simulated by PFM is considerably smoother, compared to that of LSM. On the other hand, t_{in} affects the area conservation during the time dependent computations. As shown in Fig. 2, for a given Pe, a small t_{in}/t_{dif} results in early abrupt bubble shrinkage in both methods due to the initially unstable ϕ. At a later stage, R_s takes relatively the same gradient as that for larger t_{in}/t_{dif}. Therefore, at a given diffusion coefficient, initialization step has to have enough time in order to stabilize ϕ at the initial interface. However, t_{in} must be small enough to avoid any deformation caused by pure diffusion.

The effect of diffusion coefficients (or Pe) on the shrinkage rate are presented separately for LSM and PFM in Fig. 3. In general, the area change of bubble is less than 1% up to $t_D = 150$ for the two

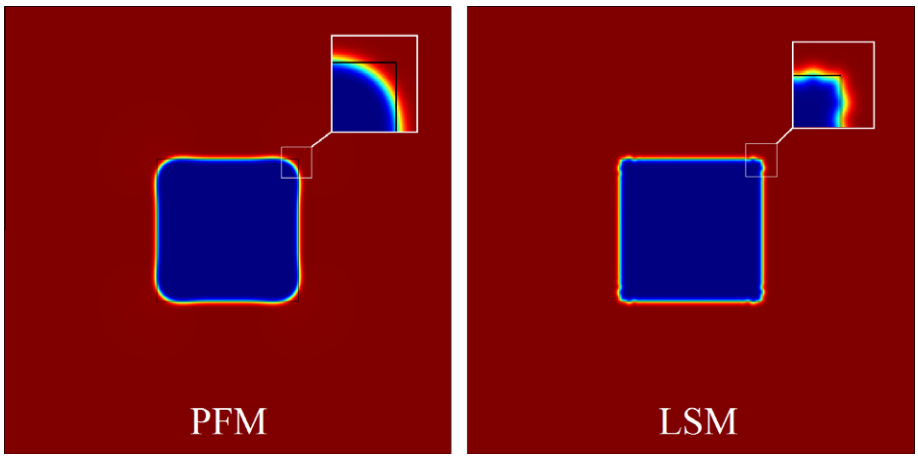

Fig. 1. The rectangular bubble profile computed by PFM and LSM at the end of the initialization step (before time dependent solving) when t_{in}/t_{dif} is large. For PFM, Pe = 7.25e5 and t_{in}/t_{dif} = 2.5. For LSM, Pe = 5.3e5 and t_{in}/t_{dif} = 5.

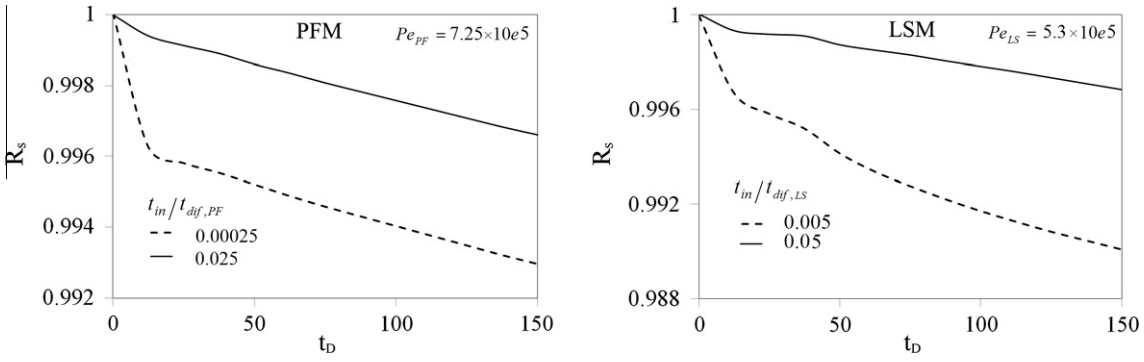

Fig. 2. Shrinkage ratio of the bubble (R_s) as a function of t_D for LSM and PFM with different t_{in}/t_{dif}.

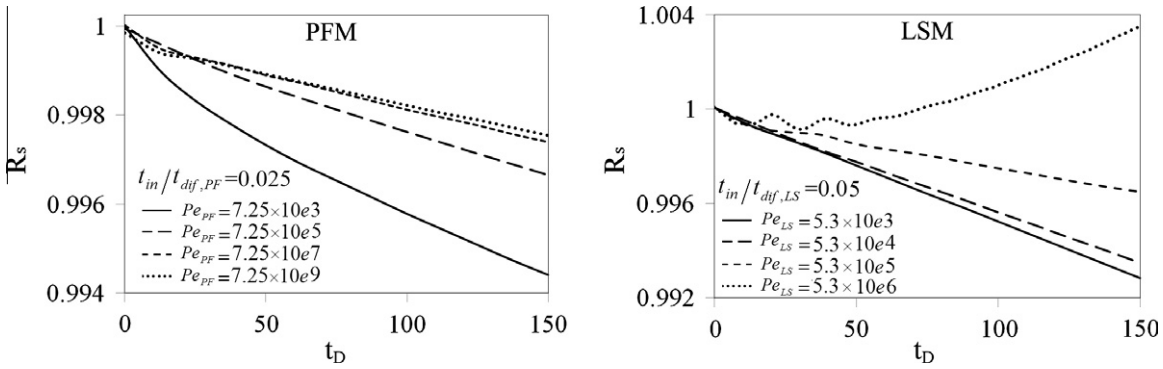

Fig. 3. Shrinkage ratio of the bubble (R_s) as a function of t_D for LSM and PFM with different Pe.

methods, however PFM shows smaller rates of shrinkage at different Pe, in comparison with LSM, i.e., PFM has better performance in conserving the bubble area. In general, as Pe increases, the rate of shrinkage decreases for the two methods. Diffusion may shift the interface contour and change the volume of the bubble as the interfacial profile evolves in a flow field (Yue et al., 2006). The diffusion effect is minimized when Pe increases. As shown in Fig. 3, as Pe increases in PFM, the rate of shrinkage converges. However for LSM, at high Pe (>5.3e5) the bubble is expanded (matrix shrinkage). This may be due to the inability of re-initialization step in keeping ϕ_{LS} across the interface at high Pe (Olsson et al., 2007).

3.2. One directional stratified two phase flow

The well-known Poiseuille flow in 2D channel is simulated using LSM and PFM. This study serves to validate and compare the methods in simulating two-phase flow with viscosity contrast. The influences of model convergence and mesh convergence on the accuracy of the results are studied. The wetting phase (phase 1) flows along the channel wall, while the nonwetting phase (phase 2) flows in the center. Standard no-slip boundary conditions are used for channel walls and fixed pressure gradient is imposed over the channel length. After a transition period, the steady state condition is achieved. There is not any considerable deformation in the

interface and the fluid currents are parallel. The following characteristic length and velocity are defined: $l_c = H$ and $u_c = \nabla P H^2/\mu_1$, where H is the channel width and ∇p is the pressure gradient in the channel. To avoid flow turbulencies, *Re* number is taken within the laminar flow regime (<2000), so the values of pressure gradient, viscosities and channel dimension are critical.

Simulations for a wide range of pressure gradients, bulk viscosities and channel widths are performed and the results are normalized with the characteristic length and velocity. Fig. 4 depicts the numerical results for $\beta = 10$ and $\beta = 0.1$. As discussed in Section 2.3, a precise diffuse-interface solution requires that the interface to be thin enough to approximate the sharp-interface limit (model convergence), and that the thin interface to be resolved by a sufficient number of grid points (mesh convergence). For the mesh convergence tests, as an initial guess, Cahn number is fixed at $Cn = 0.01$ and the mesh size (h) is varied as a function of ε. The numerical results are compared with the obtained analytical velocities from simplified Navier–Stokes equation. As shown in Fig. 4a, the predicted velocities by LSM are more sensitive to mesh size, compared to PFM for this particular case. The results for LSM at $h = 5\varepsilon$ and $\beta = 0.1$ are not shown in Fig. 4a since the velocity did not reach steady state. Mesh convergence is achieved for PFM when $h \leqslant 2.5\varepsilon$, while for LSM convergence is reached at smaller mesh size of $h \leqslant \varepsilon$. Fig. 4a demonstrates that when $Cn = 0.01$, the velocities are not accurate enough compared to analytical solution, so the interface thickness has not yet approached to the sharp limit. In order to confirm model convergence, *Cn* was reduced to 0.001. As shown in Fig. 4b, as *Cn* decreases, the predicted velocities by both methods approach the exact solutions at different viscosity ratios and they are in a good agreement with the analytical solution at $Cn = 0.001$ and $h = \varepsilon$. From Fig. 4a and b it may be concluded that the accuracy of the results for LSM and PFM is more dependent on the interface thickness, than the mesh size for this particular case. This may be due to the interdependency of the interfacial thickness and the widths of the fluids in the parallel flow. As the interface approaches sharp limit, the fluid thicknesses retain their real size and the velocity profiles approach the exact values.

In the analytical solution of the parallel two-phase flow in 2D channel, which is obtained from Navier–Stokes equation, the velocities are independent of surface tension coefficient. A sensitivity study is done to investigate the accuracy of the two methods in modeling surface tension in this two-phase flow problem. The effect of capillary number, $Ca = \mu_1 u_c/\sigma$ on two-phase velocity profiles with $\beta = 1$ in half symmetry of the channel is presented in Fig. 5. At high *Ca* (i.e. negligible surface tension), both methods predict the exact velocities. By decreasing *Ca*, PFM results remain in a good agreement with the analytical solution; however LSM results deviate from the analytical solution by predicting higher velocities. This may be due to the fundamental differences between the governing equations of LSM and PFM. In LSM, the

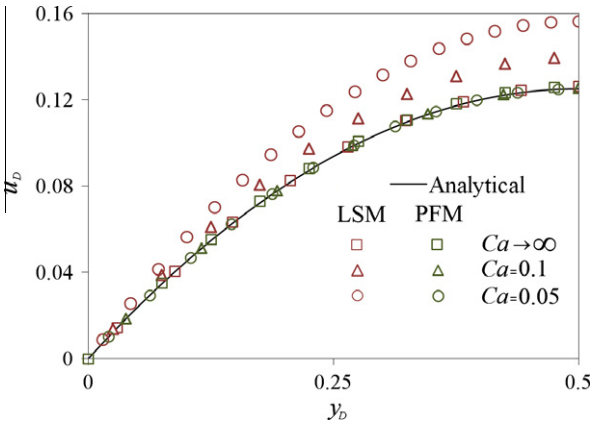

Fig. 5. The effect of *Ca* on symmetry velocity profiles obtained by LSM and PFM for stratified two-phase flow in 2D channel with equal viscosities in which the wetting phase volume fraction is 50%.

effect of surface tension is included in the definition of the interfacial body force (Eq. (6)) in Navier–Stokes equation (Eq. (4)); while in the case of PFM, surface tension coefficient does not only affect the momentum equation through interfacial force term (Eq. (7)), but also influences the evolution of the interface through chemical potential term (Eq. (2)).

3.3. Simulation of fluid flow through porous media

In this section, several 2D numerical experiments are presented to demonstrate the capabilities and limitations of the two methods in simulation of complex two-phase flow with viscosity contrast through different types of porous media.

3.3.1. Single pore model

Due to the complexity of the fluid flow through porous media, when the interface is not sharp enough or it is not resolved by enough mesh grids (i.e., the model and mesh are not converged), the results are unreliable due to the numerical distortions. In this step, a single pore is therefore selected to address the model convergence and mesh convergence. As shown in Fig. 6, the pore element consists of the circular grains with diameter of D_g, the pore throats with diameter of D_t and pore area. It is initially saturated with the phase 1 (oil). An inlet is located on the left hand side of the element, through which the phase 2 (water) is injected into the pore area at a constant velocity (u_{in}). u_{in} is taken small enough to keep the flow within the laminar regime and large enough to minimize the effect of surface tension on the flow behavior. The outlet is located on the right hand side of the element and is kept at zero pressure. No-slip boundary conditions are used for the grain

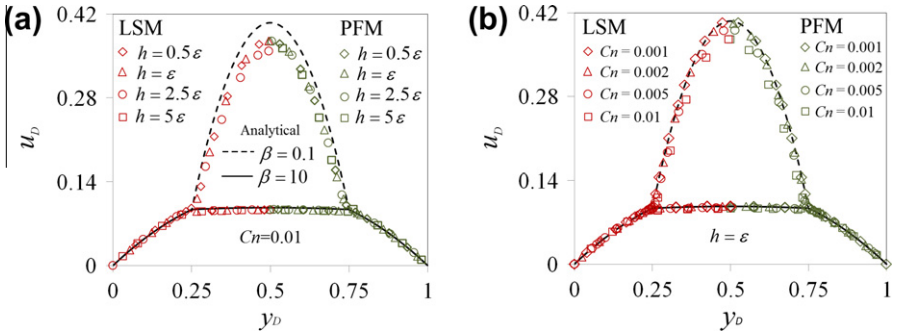

Fig. 4. Comparison of analytical and simulated profiles of dimensionless velocity versus dimensionless channel width in stratified two phase flow for $\beta = 10$ and $\beta = 0.1$ at phase 1 volume fraction of 50%. The numerical results are shown as functions of (a) mesh size with $Cn = 0.01$ and (b) *Cn* with $h = \varepsilon$.

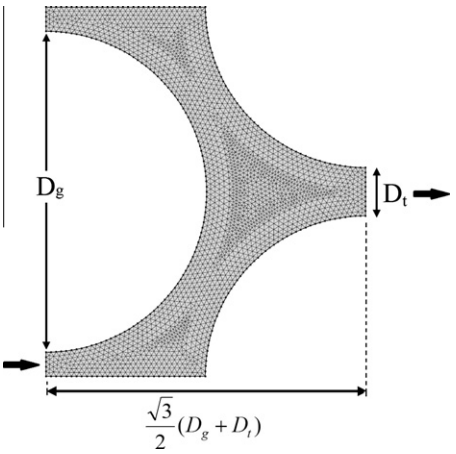

Fig. 6. The schematic of the discretized computational domain of the pore element ($h = 0.015D_g$). The dimensions of the element components and the inlet/outlet are specified.

surfaces or in other words, the fluid-grain contact angle is set to $\pi/2$ (neutral wettability). Symmetry boundary conditions are taken for the lateral sides, to extend the geometry in the lateral directions. The characteristic length and time are defined as $l_c = D_g$ and $t_c = D_g/u_{in}$, respectively. The volume fraction of water inside the element (R_v) as a function of time is numerically studied. As water flows through the element, R_v increases linearly as a function of time until water reaches the outlet (water breakthrough time). When the steady state condition is achieved, R_v is stabilized while a certain volume of the initial oil is trapped on the upper side of the element.

The viscosity ratio is set to $\beta = 10$. To confirm the mesh convergence, we set $Cn = 0.03$ and vary the mesh size from $h = 2\varepsilon$ to $h = 0.5\varepsilon$. The LSM solution did not converge at $h = 2\varepsilon$. As shown in Fig. 7, the mesh convergences in PFM and LSM are achieved when $h \leqslant 0.8\varepsilon$. Analytically, R_v is stabilized after breakthrough time, due to incompressibility of the fluids. However, both methods predict a gradual increase of R_v versus time. This is mainly due to the numerical volume shrinkage of the trapped oil. It is important to note that PFM predicts lower shrinkage compared to LSM. This is in agreement with the observations made in Section 3.1 for rectangular bubble deformation.

To confirm the model convergence, mesh size is set to $h = 0.8\varepsilon$ and Cn varies from 0.1 to 0.01 (Fig. 8). The PFM prediction converges to the sharp-interface limit when $Cn \leqslant 0.03$, while LSM needs a thinner interfacial layer ($Cn < 0.02$). The LSM results show larger variations in the tested values of Cn. This demonstrates that LSM is more sensitive to the interfacial thickness, compared to PFM. It is worth to note that the rate of volume shrinkage in both methods (especially in LSM) decreases as the interface approaches the sharp limit. Based on the above studies, the later PFM and LSM computations are performed using $Cn = 0.01$ and $h = 0.8\varepsilon$, to make sure that the interface is sharp enough and is resolved by enough mesh in both methods.

From the physical point of view, when $\beta \geqslant 1$ the displacement process is stable. However, when the viscosity of the displacing fluid is less than the displaced fluid ($\beta < 1$), physical interface instabilities occur which are known as Rayleigh–Taylor instabilities in fluid dynamics. In larger scales, this phenomenon is called fingering, which is prevalent in water-flooding of the porous media that contain oil with larger viscosity than water. The effects of β on the simulation results of PFM and LSM are studied in this section. Fig. 9 illustrates the fluid profiles at $t_D = 10$ (steady state condition) predicted by PFM and LSM with different viscosity ratios of 1, 10 and 0.1. Fig. 10 depicts R_v versus time for the two methods at different β. In general, LSM and PFM predict different steady profiles for the interface. In the case of PFM, the interface ends are stabilized perpendicular to the grain walls, in agreement with the imposed no-slip boundary condition. However, the ends of the interface predicted by LSM make are at oblique angles with the grain walls at steady condition, which means that the interface is unstable in LSM. On the other hand, LSM predicts relatively similar profiles for fluid distributions (Fig. 9) and water volume fractions (Fig. 10) at different viscosity ratios. However, PFM computations result in different fluid profile and water volume fraction when $\beta = 0.1$. As shown in Fig. 9 for PFM at $\beta = 0.1$, not only the volume of the trapped oil in the upper side of the element increases, but also small amount of oil is trapped in the lower part. This has resulted in lower R_v (or higher trapped oil) at steady conditions (Fig. 10). This means that PFM could capture the physical interface instabilities.

As mentioned in Section 2.3, the numerical solver controls the size of the time steps during the computations to converge the solution. Fig. 11 illustrates the reciprocal of time step sizes taken by the solver versus number of time steps for PFM and LSM in computation of flow when $Cn = 0.01$, $h = 0.8\varepsilon$ and $\beta = 0.1$. Although the average time step sizes are approximately the same, the amplitudes of step size fluctuations in PFM is much less than LSM. These fluctuations result in larger number of time steps for LSM (more than two times). In spite of the number of degrees of freedom for LSM which is much less than PFM (see Section 2.3), the running of LSM computations takes longer time in comparison with PFM (about 1.5 times).

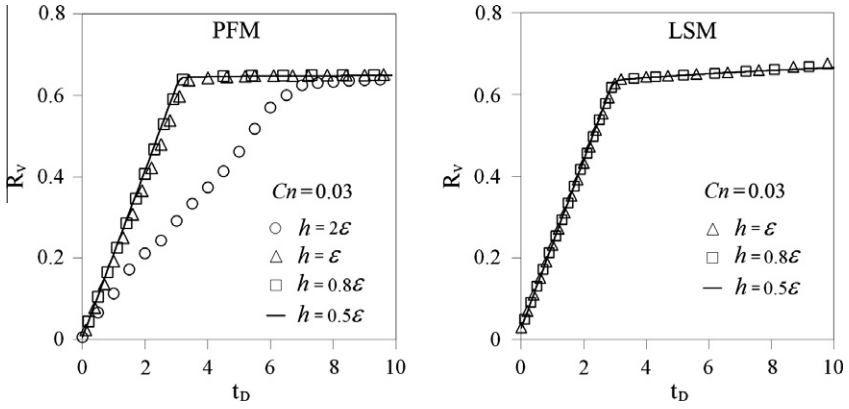

Fig. 7. Water volume fraction (R_v) as a function of dimensionless time for the pore element simulated by PFM and LSM. The convergence is studied with respect to the mesh resolution at $Cn = 0.03$.

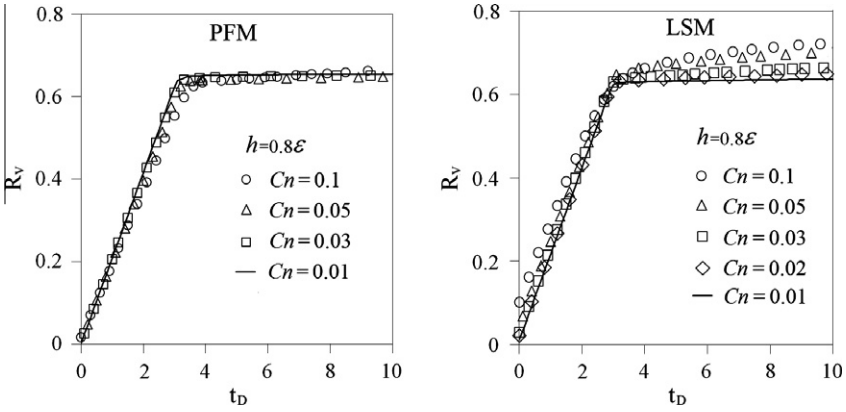

Fig. 8. Water volume fraction (R_v) as a function of dimensionless time for the pore element simulated by PFM and LSM. The convergence is studied with respect to the interfacial thickness when $h = 0.8\varepsilon$.

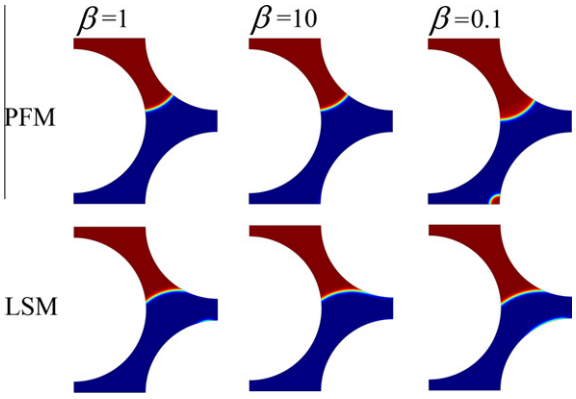

Fig. 9. Comparison between PFM and LSM predictions of two-phase flow profile through the pore element at $t_D = 10$ for three different viscosity ratios.

A slightly more complicated pore element is simulated to investigate the effects of the diffusion terms on the results of PFM and LSM. The new model is similar to the pore element that was described above; however as depicted in Fig. 12, the diameter of the upper grain is smaller ($0.8D_g$) that creates inhomogeneity (dual permeability) in the model. Another difference between the new model and the previous one is that water is injected from two inlets on the left hand side of the element, so the water currents from the inlets merge in the pore area. Computation of two interfaces while merging is one of the difficulties of two-phase flow simulation methods, especially in modeling of flow through porous media. This is more complicated if the interfaces have different profiles before merging, which the case in inhomogeneous media is. Fig. 13 shows the effects of diffusion coefficients (M_c and ω) on the results of PFM and LSM during interface merging. The viscosity ratio is $\beta = 1$. As shown in Fig. 13, the PFM predicted interfaces are stable (perpendicular to the walls) at different mobility values during the merging. However, the LSM interfaces are not normal to the walls before and after merging, which demonstrates the instability of the interfaces. In the case of PFM, it is observed that before merging, the interface profiles are not a function of M_c at 1 and 0.01. However the LSM results demonstrate that the forms of the interfaces (especially the upper one) are dependent on ω. For both methods higher diffusion coefficient has resulted in a more realistic interface merging. This is more evident in the case of LSM, in which a numerical intermediate phase is formed during merging when $\omega = 0.01$. From a physical point of view, since $\beta = 1$, the pore area is fully flooded by water; however it is observed that LSM predicts small trapped oil in vicinity of the grain wall, which is due to the numerical instabilities originated by unstable interfaces. It is worth noting that this small trapped oil shrinks gradually with time and eventually disappears, not shown here, in agreement with the previous LSM results. The diffusion coefficients in the coming simulations are set based on the sensitivity analysis performed in this section and Section 3.1.

3.3.2. Homogenous porous medium

The homogenous porous medium is simulated by subtracting the homogenously distributed circular grains from a rectangular domain with the area of $0.015 \times 0.0046\ m^2$. The circular grains are represented by an equilateral triangular array ($[16 \times 5]$). The

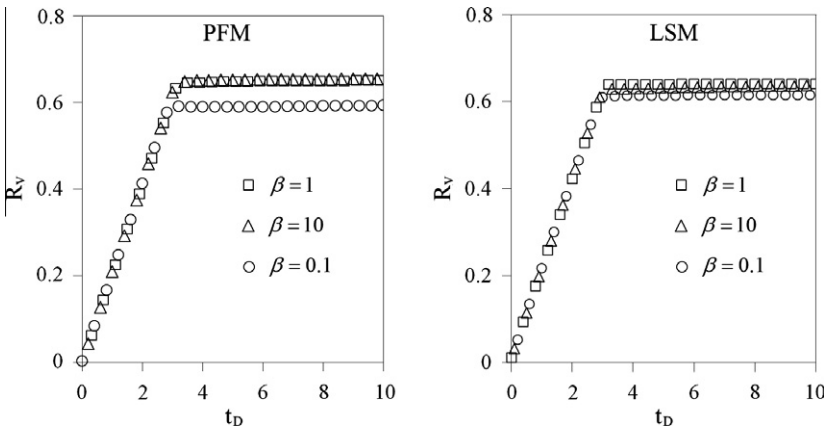

Fig. 10. Comparison between PFM and LSM predictions of water volume ratio (R_v) in the pore element versus t_D for three different viscosity ratios.

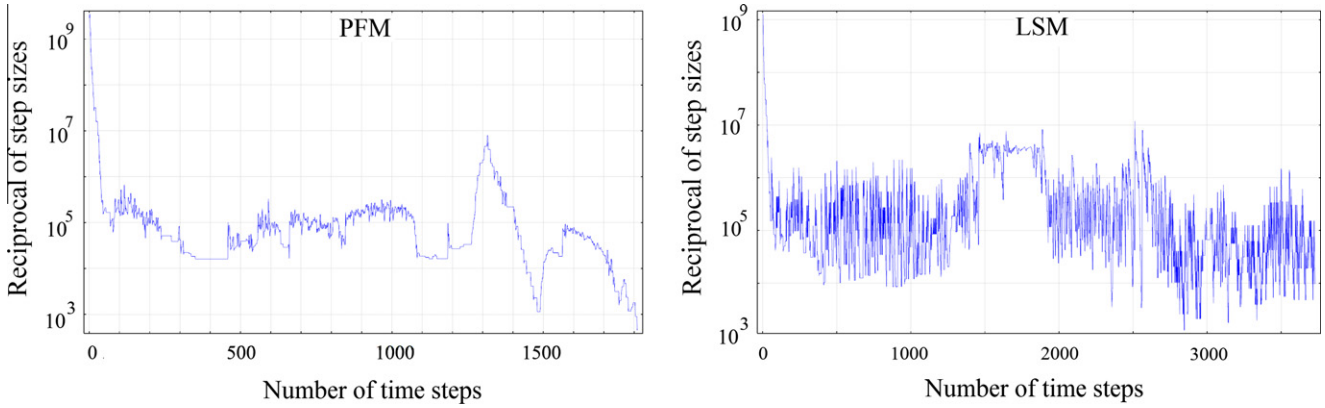

Fig. 11. Comparison between PFM and LSM history of reciprocal of step sizes versus number of time steps in computation of flow through the single pore element.

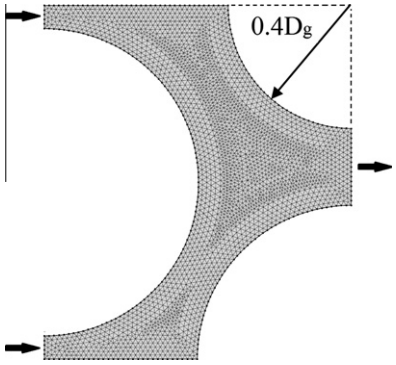

Fig. 12. The schematic of the discretized computational domain of the inhomogeneous pore element ($h = 0.015D_g$).

same as the pore element, no-slip and symmetry boundary conditions are used for the grain walls and the lateral sides, respectively. The model is initially saturated with the oil and the water is injected with constant velocities through the inlets on the left hand side of the model. The outlets are located on the other side of the domain and their pressure is set to zero. Water and oil densities are set to 1000 kg/m^3 and the interfacial tension coefficient is set to 0.04 N/m.

The grain diameter (D_g) and the throat size (D_t) determine the void fraction (porosity) of the medium. Experimental studies show that there is a relationship between the medium fluid flow properties, porosity and surface area. The Kozeny–Carman formulation (Chilingar et al., 1963) is a well-known empirical correlation that relates the medium absolute permeability to the porosity and the average grain size of a pore volume. This correlation can be stated as $k = CD_g^2\varphi^3/(1-\varphi)^2$, where k is the absolute permeability, φ is the porosity of the medium and C is the Kozeny–Carman constant that depends on the type of porous medium. When one fluid flows through porous medium, absolute permeability is obtained by $k = Q\mu/(A\nabla p)$, where A is the medium cross section area (in 2D models it is corresponding to the width of the medium), ∇p is the pressure gradient in the medium and Q is the liquid flow rate that is calculated by integrating the steady fluid velocity on the outlet. The absolute permeability versus Kozeny–Carman formulation is plotted in Fig. 14 for the media with different porosities simulated by the two methods. Fig. 14 shows a linear relationship between the absolute permeability and Kozeny–Carman relation, which confirms the consistency of the numerical models with the existing empirical correlation. The slope of the line determines the Kozeny–Carman constant for this medium.

A uniform homogenous medium with an obstacle is constructed using LSM and PFM to compare the effects of flow disturbance and viscosity contrast on the results of the two methods. In this medium we set $D_g = 0.001$ m and $D_t = 0.00015$ m. The domain area, pore network distributions and boundary conditions are as described above. The medium porosity is obtained as $\varphi = 35\%$. Fig. 15 depicts the geometry of the domain, in which a small obstacle (perturbation) is simulated between two grains at the beginning of the medium. For the flow through porous media, the critical values

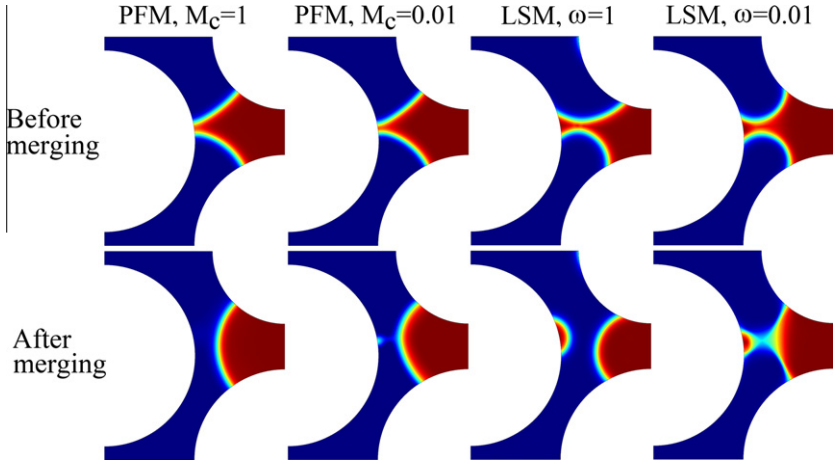

Fig. 13. The interface profiles before and after merging in inhomogeneous pore element, simulated by PFM and LSM with different diffusion coefficients.

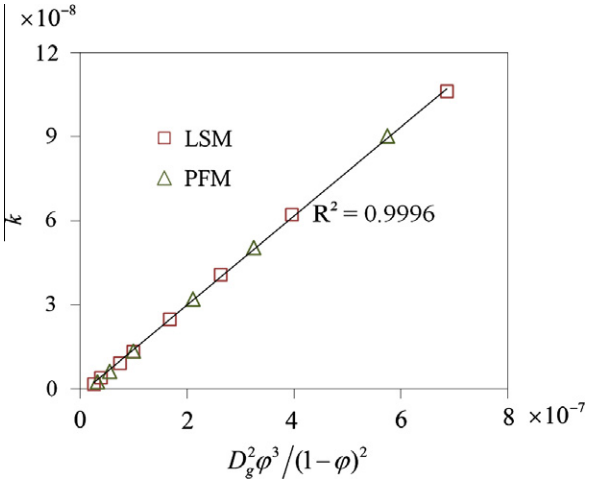

Fig. 14. Absolute permeability as a function of Kozeny–Carman relation for homogenous porous media, simulated by LSM and PFM.

of Reynolds number at the onset of non-laminar flow, according to the reported empirical and numerical experiments, range between 1 and 10 (Hassanizadeh and Gray, 1987). The critical Re of 2 is used in this work. The injection velocity (u) is set low enough to mimic the laminar regime. On the other hand, it is set high enough to minimize the effect of the interfacial tension on the flow behavior (High Ca). Hence the flow pattern depends on viscosity ratio more than on the interfacial tension. Water and oil viscosities are set to $\mu_w = 0.001$ and $\mu_o = 0.02$ Pa s, respectively. As described in Section 3.3.1, when $\beta \ll 1$, the interface instabilities may cause fingering phenomenon. Displacement of viscous oil by a less viscous solvent is inherently unstable, even when the medium is homogeneous. The presence of heterogeneities (such as obstacle) inevitably influences the formation of viscous fingering (Araktingi and Orr, 1993). The obstacle is simulated in this problem as an initial flow perturbation to initiate the instabilities. This perturbation creates a kind of anisotropy in the medium.

Fig. 16 compares PFM and LSM predicted phase profiles and flow streamlines just after the time when water passes the obstacle ($t_D = 2.7$). Small amount of oil is trapped behind the obstacle. As was noticed in the single pore element (Fig. 9), different interface profiles are predicted by the methods around the trapped oil. It is possible to observe unstable interfaces (with oblique angles with the grain walls) in the result of LSM, similar to what was observed in the pore element. Water, which is injected from five inlets, is forced to pass through three pore throats. In PFM the water streamlines are concentrated on the middle throat, so the velocity in the middle throat is higher than the lateral ones at this time. However, LSM predicts higher velocities for the two lateral throats. As demonstrated in Fig. 17, the pressure distributions at $t_D = 2.7$ are exactly the same for the two methods, except the pressure of water. PFM simulates a lower water pressure (~750 Pa), compared to LSM (~1000 Pa), maybe due to their difference in implementation of surface tension (see Section 3.2). In the PFM predicted profile, the maximum pressure is for the trapped oil, which is physically more realistic.

The preliminary differences between the results of the two methods lead to quite different fluid profiles in later times. The fluid distribution profiles at breakthrough times are compared in Fig. 18. The water breakthrough time in PFM simulated model is $t_D = 25$, which is earlier than the LSM breakthrough time ($t_D = 30$) due to different predicted water profiles. Both methods demonstrate the water fingers, which are initiated by the obstacle. However the predicted flow patterns are completely different for PFM and LSM, in terms of the number, sizes and directions of the fingers. PFM simulates two relatively parallel thick fingers which are initially separated around the obstacle and flow with relatively the same velocities toward the outlets. In LSM predicted profile, the water streams are joined together just after the perturbation, then sets of small fingers are formed which propagate in various directions of anisotropic medium. According to the literature laboratory and computational studies (e.g. Araktingi and Orr, 1993; Tang and Wei, 1996 Riaz et al., 2007; Buchgraber et al., 2011), when a low viscosity fluid is injected in a medium which is saturated with a high viscosity fluid, after a while, several large fingers initiate that spread at their tips toward the outlet. Later at longer distances, the finger tips may become unstable and split into several smaller fingers. Our numerical model has small dimensions, and based on the previous studies, just few large fingers which are directed toward the outlets are expected to be formed. It may be concluded that the formed fingers in PFM are more physically realistic, while the special fingering phenomenon observed in the LSM results seems to be due to the numerical instabilities. Fingering causes an early water breakthrough, which results in a low sweep efficiency of the displacement process. After water breakthrough, the injected water flows through the fingers directly to the outlets, so some parts of the media remain unswept. The earlier water breakthrough time in PFM results in prediction of lower sweep efficiency, compared to LSM. Fig. 19 compares the LSM and PFM predicted volume fraction of injected water in the medium and average pressure gradients between the inlets and the outlets as functions of time. The pressure gradient (∇p) is nondimensionalized by the characteristic pressure gradient (∇p_c) which is defined as the pressure gradient when water is the only flowing fluid inside the medium. As shown in Fig. 19, R_v increases linearly for both methods due to the constant injection velocity up to breakthrough time. For PFM after the breakthrough time of the first finger ($t_D = 25$), the second finger still moves toward the outlet. Then R_v is stabilized and no more oil is produced. For LSM as water breakthroughs from the upper outlet (at $t_D = 30$), not only no more oil is produced, but also the water area starts to shrink mainly due to the numerical instabilities of the predicted interfaces, hence R_v

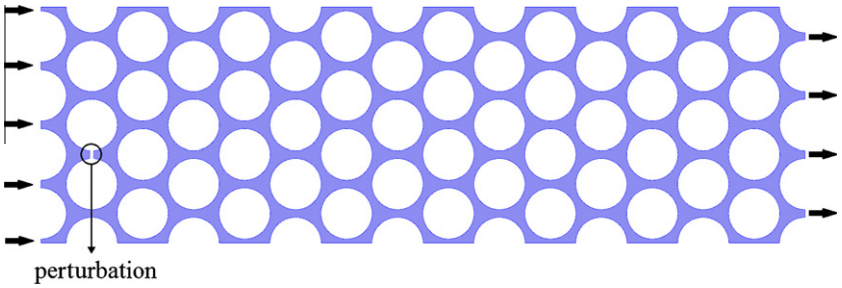

Fig. 15. The schematic of the geometry of the homogenous medium with obstacle. The inlets/outlets and the obstacle are specified.

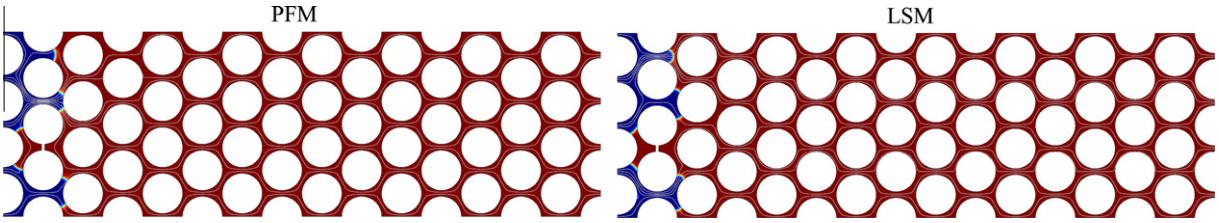

Fig. 16. Comparison between the phase distributions and flow streamlines in homogenous porous medium at $t_D = 2.7$, simulated by PFM and LSM.

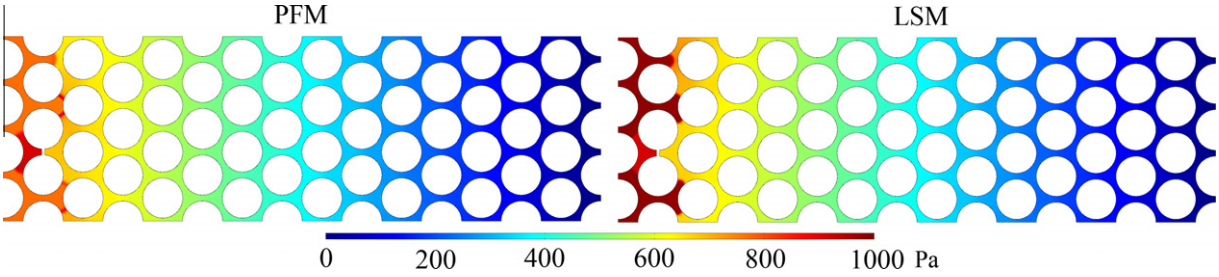

Fig. 17. Comparison between the pressure profiles in homogenous porous medium at $t_D = 2.7$, simulated by PFM and LSM.

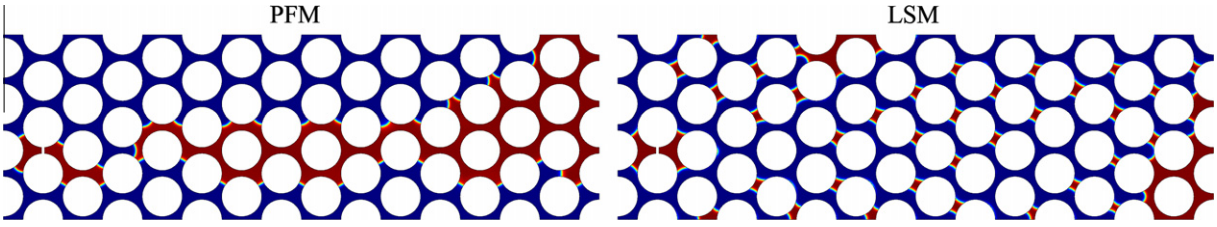

Fig. 18. Comparison between the phase distributions in homogenous porous medium at water breakthrough time, simulated by PFM and LSM.

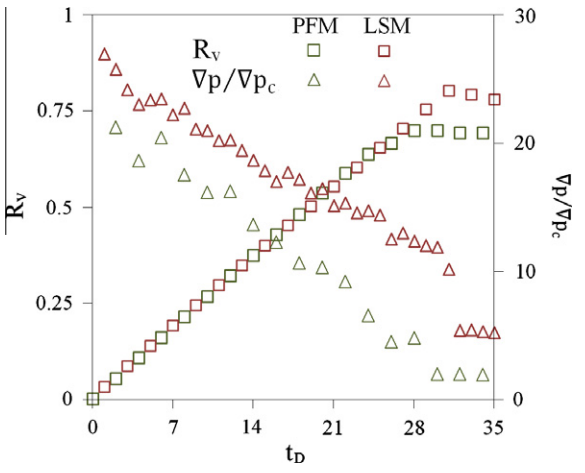

Fig. 19. Volume fraction of injected water (R_v) and dimensionless average pressure gradient between inlets and outlets versus time in homogenous medium simulated by PFM and LSM.

decreases. Analytically, the pressure gradient at $t_D = 0$ (∇p_0) can be calculated as the pressure gradient when the medium is fully saturated with oil ($\nabla p_c/\beta$) plus surface tension pressure ($\approx 2\sigma/D_g$). For the above given β, σ and D_g, the initial dimensionless pressure ($\nabla p_0/\nabla p_c$) is approximately obtained as 22, which is in agreement with PFM initial pressure gradient (Fig. 19). Due to the lower viscosity of water compared to oil, as water is injected, the pressure gradient inside the medium declines. As shown in Fig. 18, water moves straightly toward the outlet in PFM predicted profile. So the water front in PFM is faster in approaching the outlet, compared to LSM; hence the inlet pressure (and pressure gradient) decreases with a higher rate for PFM. After breakthrough time, the flow happens only through the water path, so the pressure gradient jumps to a constant lower value which is equal to ∇p_c, hence the dimensionless pressure gradient is analytically obtained as 1, in agreement with PFM result.

The domain of the homogenous porous medium with obstacle was discretized using 101,117 mesh grids. The number of degrees of freedom in time dependant solving of this numerical model was 898009 and 678211 for PFM and LSM, respectively. As observed before in Section 3.3.1, despite the lower degrees of freedom of LSM, the number of time steps in the solution of LSM was 18632 which is approximately four times that of PFM (4795). The large number of step sizes result in a considerably longer running time for LSM simulation which was 120 h, compared to 40 h for PFM, on a system with 2.67 GHz CPU and 16 GB RAM.

3.3.3. Dual-permeability porous medium

The influence of permeability contrast on the water-flooding process is investigated in this section. The dual-permeability medium (Fig. 20) is simulated by decreasing the diameter of the grains in one side of the homogenous medium that was described in the previous section. The thickness of high permeable layer is 0.0017 m. The grain diameter and throat size in high permeable region are 0.0008 and 0.00035 m, respectively. The permeability ratio between the high permeable layer and the bulk is approximately 10.

From the physical point of view, the injected water tends to flow through high permeable layer due to the lower flow resistivity of this

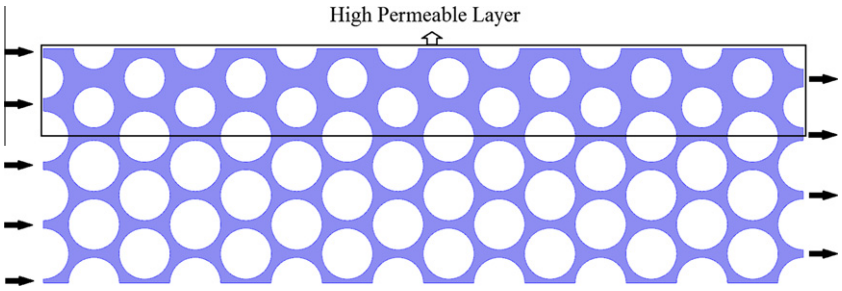

Fig. 20. The schematic of the geometry of dual-permeability medium. The inlets/outlets and the high permeable layer are specified.

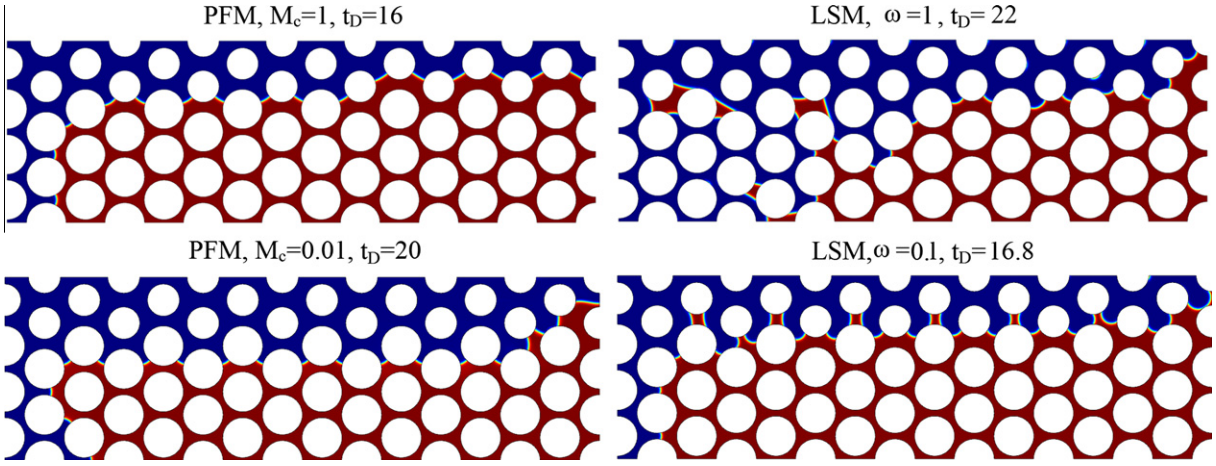

Fig. 21. Comparison between the fluid distributions predicted by PFM with M_c = 1 and 0.01and LSM with ω = 1 and 0.1 at water breakthrough times.

layer compared to the low permeable one. The low permeable zone remains unswept, except small parts close to the inlets, where the injected water is stabilized. The effects of M_c and ω on two-phase flow in a single pore were studied in Section 3.3.1. To better comprehend the influences of the diffusion coefficients (M_c and ω), a study is performed in complicated dual-permeability medium. The fluid distributions predicted by PFM and LSM for dual-permeability model are compared in Fig. 21. The comparison is made on two different diffusion coefficients for each method at water breakthrough time when $\mu_w = \mu_o$ = 0.001 Pa s. Although in all the simulations, an earlier water breakthrough is observed in high permeable layer, the profiles of the water and the breakthrough times are different. As depicted in Fig. 21, the diffusion coefficients considerably affect the results in both methods, especially for LSM. In the case of PFM, as mentioned in Section 2.3, M_c has to be large enough to retain a constant interfacial thickness and small enough to keep the convective motion. The results for both M_c values (1 and 0.01) show a more or less constant interfacial thickness during fluid propagations. In other words this range of M_c is large enough to properly diffuse the interface. The different water profiles predicted by PFM with different M_c values are mainly due to the influence of M_c on the convective motion. Lower M_c has resulted in easier water–oil displacement hence higher water volume fraction in high permeable zone and later breakthrough time. Comparison of the numerical results with experimental observations is a possible way to find the proper diffusion coefficient. Similar to the previous sections, the first observation in the results of LSM is unstable interfaces in contact with the no-slip grain walls. Moreover, it is possible to see that ω considerably affects the LSM predicted water profiles. When ω = 1, LSM computes a larger water swept area in low permeable zone compared to what is physically expected. By decreasing ω to 0.1, the LSM predicts a more realistic water profile, similar to PFM results. However several volumes of trapped oil appear in high permeable zone, which are mainly due to a lower diffusion coefficient that makes it difficult for the interface to merge, as discussed in Section 3.3.1. Since the water profiles and breakthrough times predicted by PFM and LSM are relatively similar when M_c = 1 and ω = 0.1, the later studies are done using these cases.

The average pressure gradients in high permeable layer and water volume fraction in the medium as a function of time are compared for PFM and LSM in Fig. 22. The pressure gradient (∇p) is nondimensionalized by the characteristic pressure gradient (∇p_c) which is defined here as the pressure gradient in high perme-

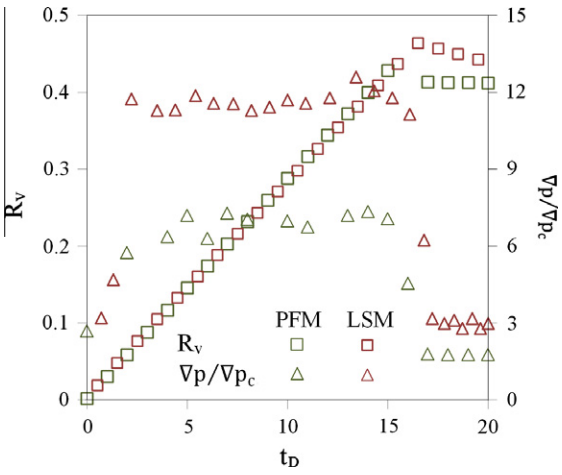

Fig. 22. Volume fraction of injected water (R_v) in dual-permeability medium and dimensionless average pressure gradient in high permeable layer versus time simulated by PFM with M_c = 1 and LSM with ω = 0.1.

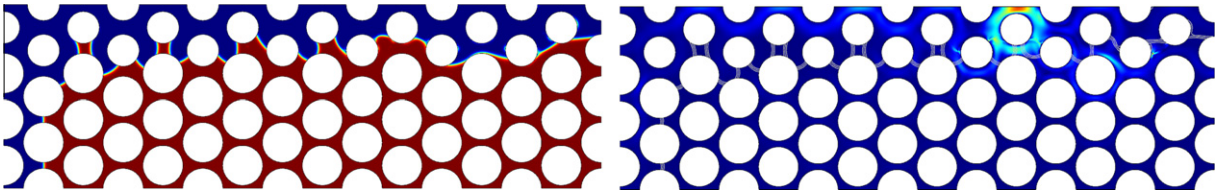

Fig. 23. Snap shots of fluid distributions (to the left) and velocity field (to the right) at $t_D = 18$ (after water breakthrough time) predicted by LSM with $\omega = 0.1$.

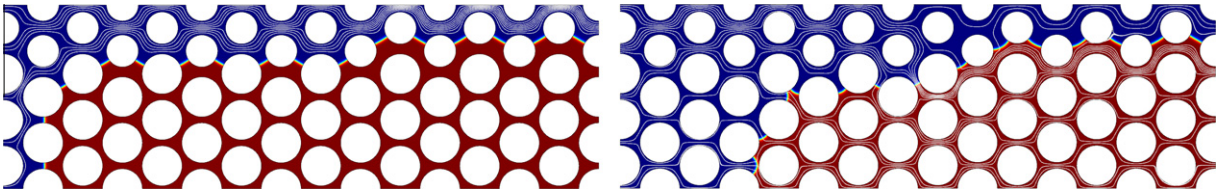

Fig. 24. Fluid distributions and flow streamlines at $t_D = 20$ (to the left) and $t_D = 30$ (to the right) simulated by PFM with $M_c = 1$. Water viscosity is enhanced at $t_D = 25$.

able layer when water is the only flowing fluid inside the medium. After a transient time, the pressure gradients in both methods get relatively constant values before breakthrough time due to equal viscosities of oil and water. LSM predicts higher pressure gradients in high permeable layer, compared to PFM. The analytical values for the dimensionless pressure gradient in high permeable layer before and after breakthrough time are 6 and 1, respectively (based on the approximation made in Section 3.3.2). The PFM predicted pressures are in a good agreement with the analytical values. As shown in Fig. 22, unlike PFM which is successful in keeping a stable water profile after breakthrough time, the LSM predicted water volume fraction declines after breakthrough time which again confirms the area shrinkage as well as instability of no-slip boundary conditions in LSM. Fig. 23 demonstrates the fluid distribution and velocity field computed by LSM just after breakthrough time ($t_D = 18$). Fig. 23 also shows that the simulated trapped oils (as demonstrated in Fig. 21 for LSM with $\omega = 0.1$) disappear in a short time after breakthrough, due to unstable interface deformations. The velocity profile clearly illustrates high velocity spots around the unstable interface, which are due to the numerical effects and cause nonrealistic deformations.

It is possible to recover the remaining oil by enhancing the water phase viscosity after breakthrough time. Water viscosity is enhanced to 0.04 Pa s at $t_D = 25$ by defining a step function. Fig. 24 compares the fluid distributions and flow stream lines predicted by PFM at two different times before and after viscosity enhancement. After water breakthrough, all the injected water goes directly through the water path and does not sweep the remaining oil. By enhancing the water viscosity, the resistivity of the water path increases, hence water is diverted toward the low permeable areas and sweeps the oil. With this viscosity ratio, finally almost entire oil in the medium is fully displaced by water.

Similar to what has been discussed in more details for the homogenous model, the number of time steps taken by solver in simulation of dual-permeability medium with LSM was more than seven times that of PFM. Consequently, the LSM simulation running time took more than five times longer than PFM for this model.

4. Conclusions

Different 2D models are simulated by conservative level set method (LSM) and Cahn–Hilliard phase field method (PFM), using a robust finite element solver to evaluate and compare the methods based on their running time, accuracy and ability to capture physical phenomena related to flow in porous media. The assessment enables us to select a suitable model for the future works in enhancing oil recovery, in which fluids having different viscosities flow through dual-permeability porous media.

The study of rectangular bubble deformation shows that PFM better conserves the area compared to LSM; however initialization time and diffusion coefficient are important factors that affect the rate of area shrinkage in both methods. Longer initialization time and higher *Pe* (lower diffusion coefficients) result in lower rate of area shrinkage. It is demonstrated that PFM better handles the surface tension created parasite currents. Parallel two phase flow through 1D channel serves to study the effects of model convergence and mesh convergence on accuracy of the methods. It is concluded that the results of the two methods are almost insensitive to the mesh sizes in this particular problem, while the interface thickness plays an important role in the accuracy of the results, when compared with the analytical solution. The model convergence is not achieved even at $Cn = 0.006$ in both methods due to interdependency of the fluid thicknesses and interface thicknesses in parallel flow. The study of surface tension effect on parallel flow demonstrated that PFM more accurately predicts the fluid velocities at different capillary numbers.

To verify the influences of model convergence, mesh convergence and diffusion coefficients on the flow through porous media, two different single pore element models are studied. The results show that LSM needs thinner interface to be converged, compared to PFM, so that the PFM model convergence takes place at $Cn = 0.03$, while LSM needs $Cn = 0.01$. The results of model convergence and mesh convergence analysis in single pore element are used in simulating more complicated two-phase flow in porous media. PFM shows that is able to capture the Rayleigh–Taylor instabilities in single pore element. The interface merging process is also easier handled by PFM. Diffusion coefficients, including mobility (M) and re-initialization parameter (ω) affect the interface merging in PFM and LSM, respectively. Lower diffusion coefficient results in more difficult interface merging, especially for LSM. LSM has also difficulty in modeling stable interfaces around the no-slip walls (grains). The unstable interfaces together with high rate of area shrinkage result in physically unrealistic behaviors in the LSM results.

The effects of viscosity and permeability contrasts were studied by simulating homogenous medium containing an obstacle and dual-permeability porous medium. Both methods captured the main phenomena, including fingering and early water breakthrough due to viscosity and permeability contrasts. How-

ever, the details of PFM predictions, such as pressure gradient in the medium, fingering shapes and numbers and water profile after breakthrough time are more realistic compared to the analytical values and the experimental observations. The main drawback of LSM is that it did not capture a stable water profile after breakthrough time. Furthermore, in a specific simulation, LSM needs smaller time steps, hence larger number of time steps to converge the model solutions, so typically the LSM simulation running times are considerably longer than PFM, e.g. approximately three and five times in simulation of homogenous and dual-permeability porous media, respectively.

It is concluded that PFM, which is a physically originated method, is more efficient in simulation of complex two-phase flow through porous media. It produces more accurate results in shorter times, compared to LSM.

Acknowledgments

Authors acknowledge Dong Energy Company, Norway for the financial support and COMSOL support center for their technical recommendations in programming.

References

Araktingi, U.G., Orr, F.M., 1993. Viscous fingering in heterogeneous porous media. SPE Adv. Technol. Ser. 1, 71–79.
Badalassi, V.E., Cenicerob, H.D., Banerjee, S., 2003. Computation of multiphase systems with phase field models. J. Comput. Phys. 190, 371–397.
Blunt, M.J., 2001. Flow in porous media, pore-network models and multiphase flow. Curr. Opin. Colloid Interface Sci. 6, 197–207.
Bogdanov, I., Jardel, S., Turki, A., Kamp, A., 2010. Pore scale phase field model of two phase flow in porous medium. In: Annu. COMSOL Conf., Paris, France.
Buchgraber, M., Clemens, T., Castanier, L.M., Kovscek, A.R., 2011. A microvisual study of the displacement of viscous oil by polymer solutions. SPE Reserv. Eval. Eng. 14, 269–280.
Cahn, J.W., Hilliard, J.E., 1958. Free energy of a nonuniform system. J. Chem. Phys. 28, 258–267.
Chilingar, G., Main, R., Sinnikrot, A., 1963. Relationship between porosity, permeability and surface area of sediments. J. Sediment. Petrol. 33, 759–765.
Chiu, P.H., Lin, Y.T., 2011. A conservative phase field method for solving incompressible two phase flows. J. Comput. Phys. 230, 185–204.
COMSOL Multiphysics User's Guide, 2011. Version 4.2, Comsol Inc.
Donaldson, A.A., Kirpalani, D.M., Macchi, A., 2011. Diffuse interface tracking of immiscible fluids: improving phase continuity through free energy density selection. Int. J. Multiphase Flow 37, 777–787.
Dupont, J.B., Legendre, D., 2010. Numerical simulation of static and sliding drop with contact angle hysteresis. J. Comput. Phys. 229, 2453–2478.
Feng, J.J., Liu, C., Shen, J., Yue, P., 2005. An energetic variational formulation with phase field methods for interfacial dynamics of complex fluids: advantages and challenges. In: Maria-Carme, T., Eugene, M. (Eds.), Modeling of Soft Matter, the IMA Volumes in Mathematics and Its Applications, vol. 141. Springer, New York, pp. 1–26.
Hassanizadeh, M., Gray, W., 1987. High velocity flow in porous media. Transport Porous Med. 2, 521–531.
Hirt, C.W., Nichols, B.D., 1981. Volume of fluid (VOF) method for the dynamics of free boundaries. J. Comput. Phys. 39, 201–225.
Jacqmin, D., 1999. Calculation of two-phase Navier-Stokes flows using phase field modeling. J. Comput. Phys. 155, 96–127.
Lafaurie, B., Nardon, C., Scardovelli, R., Zaleski, S., Zanetti, G., 1994. Modeling merging and fragmentation in multiphase flows with SURFER. J. Comput. Phys. 113, 134–147.
Liu, C., Shen, J., 2003. A phase field model for the mixture of two incompressible fluids and its approximation by a Fourier-spectral method. Physica D 179, 211–228.
Olsson, E., Kreiss, G., 2005. A conservative level set method for two phase flow. J. Comput. Phys. 210, 225–246.
Olsson, E., Kreiss, G., Zahedi, S., 2007. A conservative level set method for two phase flow II. J. Comput. Phys. 225, 785–807.
Osher, S.J., Sethian, J.A., 1988. Front propagating with curvature dependent speed: algorithms based on Hamilton–Jacobi formulations. J. Comput. Phys. 79, 12–49.
Qin, R.S., Bhadeshia, H.K., 2010. Phase field method. Mater. Sci. Technol. 26, 803–811.
Ramstad, T., Øren, P.E., Bakke, S., 2009. Simulation of Two Phase Flow in Reservoir Rocks using a Lattice Boltzmann Method. ATCE, New Orleans, Louisiana, USA.
Renardy, Y., Renardy, M., 2002. PROST: a parabolic reconstruction of surface tension for the volume of fluid method. J. Comput. Phys. 183, 400–421.
Riaz, A., Tang, G.Q., Tchelepi, H.A., Kovscek, A.R., 2007. Forced imbibition in natural porous media: comparison between experiments and continuum models. Phys. Rev. E 75, 036305.
Shepel, S.V., Smith, B.L., 2006. New finite-element/finite-volume level set formulation for modelling two-phase incompressible flows. J. Comput. Phys. 218, 479–494.
Smereka, P., Sethian, J.A., 2003. Level set methods for fluid interfaces. Annu. Rev. Fluid Mech. 35, 341–372.
Succi, S., 2001. The Lattice Boltzmann Equation for Fluid Dynamics and Beyond. Clarendon Press, Oxford.
Sussman, M., Puckett, E., 2000. A coupled level set and volume of fluid method for computing 3d and axisymmetric incompressible two-phase flows. J. Comput. Phys. 162, 301–337.
Sussman, M., Almgren, A.S., Bell, J.B., Colella, P., Howell, L.H., Welcome, M.L., 1999. An adaptive level set approach for incompressible two-phase flows. J. Comput. Phys. 148, 81–124.
Tang, S., Wei, Z., 1996. Laboratory experiment and numerical simulation on viscous fingering. Commun. Nonlinear Sci. Numer. Simul. 1, 11–15.
Unverdi, S.O., Tryggvason, G., 1992. A front tracking method for viscous, incompressible, multiphase flows. J. Comput. Phys. 100, 25–37.
Valvatne, P.H., Blunt, M.J., 2004. Predictive pore-scale modeling of two-phase flow in mixed wet media. Water Resour. Res. 40, W07406. http://dx.doi.org/10.1029/2003WR002627.
van der Waals, J.D., 1979. The thermodynamic theory of capillarity under the hypothesis of a continuous density variation. J. Stat. Phys. 20, 197–245.
Wheeler, A.A., Ahmad, N.A., Boettinger, W.J., Braun, R.J., McFadden, G.B., Murray, B.T., 1995. Recent developments in phase-field models of solidification. Adv. Space Res. 16, 163–172.
Young, T., 1805. An essay on the cohesion of fluids. Philos. Trans. Roy. Soc. London, Ser. 95, 65–87.
Yue, p., Feng, J.J., Liu, C., Shen, J., 2004. A diffuse interface method for simulating two-phase flows of complex fluids. J. Fluid Mech. 515, 293–317.
Yue, P., Zhou, C., Feng, J.J., Ollivier-Gooch, C.F., Hu, H.H., 2006. Phase-field simulations of interfacial dynamics in viscoelastic fluids using finite elements with adaptive meshing. J. Comput. Phys. 219, 47–67.
Zhou, C., Yue, P., Feng, J.J., Ollivier-Gooch, C.F., Hu, H.H., 2010. 3D phase-field simulations of interfacial dynamics in Newtonian and viscoelastic fluids. J. Comput. Phys. 229, 498–511.